Geophysical Research Letters

RESEARCH LETTER
10.1029/2024GL110637

Toward Comprehensive Understanding of Air-Sea Interactions Under Tropical Cyclones: On the Importance of High Resolution and Multi-Modal Observations

Clément Combot[1,2], **Alexis Mouche**[1], **Clément de Boyer Montegut**[1], and **Bertrand Chapron**[1]

[1]Laboratoire d'Océanographie Physique et Spatiale, Institut Français de Recherche pour l'Exploitation de la Mer, Plouzané, France, [2]Faculty of Environmental Earth Science, Hokkaido University, Sapporo, Japan

Key Points:

- Residual sea surface height anomalies from the cold wakes of Tropical Cyclones are analyzed using a multi-modal approach at global scale
- A scaling law provides a robust interpretation of the baroclinic response to given ocean stratification and forcing conditions
- High resolution measurements are found critical to correctly anticipate the SSHA amplitudes with localized pre-storm ocean stratification

Supporting Information:

Supporting Information may be found in the online version of this article.

Correspondence to:

C. Combot,
clement.combot@ifremer.fr

Citation:

Combot, C., Mouche, A., de Boyer Montegut, C., & Chapron, B. (2024). Toward comprehensive understanding of air-sea interactions under tropical Cyclones: On the importance of high resolution and multi-modal observations. *Geophysical Research Letters*, *51*, e2024GL110637. https://doi.org/10.1029/2024GL110637

Received 6 JUN 2024
Accepted 11 SEP 2024

Author Contributions:

Conceptualization: Clément Combot, Alexis Mouche, Bertrand Chapron
Data curation: Alexis Mouche, Clément de Boyer Montegut
Formal analysis: Clément Combot
Investigation: Clément Combot
Methodology: Clément Combot, Clément de Boyer Montegut, Bertrand Chapron
Supervision: Alexis Mouche, Clément de Boyer Montegut, Bertrand Chapron
Validation: Clément Combot, Alexis Mouche, Clément de Boyer Montegut, Bertrand Chapron

Abstract The three-dimensional structure of the Tropical Cyclone's baroclinic wake is synthesized as an averaged baroclinic-dominant response of the upper ocean. The resulting persisting sea surface depression can easily be monitored using the present-day altimeter constellation. Following a semi-empirical framework, these baroclinic wake signatures are linked to the inner core TC dynamic and the ocean stratification. To collect these fine-scale parameters, spaceborne SAR instruments and Argo fleet are used, to precisely capture the maximum wind region and the irregularities of the ocean vertical structure. This combination of high-resolution information is found paramount to fully capture the modulation of sea surface height anomalies, and its mean trend, especially for major hurricanes. Baroclinic signatures mostly range around 10–20 cm and peak at 40 cm. Deeper anomalies correspond to barotropic response, removed from the present analysis.

Plain Language Summary In the wakes of Tropical Cyclones (TCs), sea surface depressions of about 10 cm appear. These TC signatures are persistent enough to be easily monitored by the current fleet of altimeter instruments. A measured sea surface height anomaly integrates and reduces the air/sea interactions during the TC passage into a single observable metric. It mostly encodes the cyclonic wind forcing and the interior ocean state. A broad constellation of remote sensing and in-situ instruments has been gathered to compile 200 cyclonic episodes, collecting a wide range of TC sizes, intensities, and translation speeds together with oceanic conditions. A synthetic relationship is found to robustly predict most observed sea surface height anomalies. Moreover, when high-resolution information is available to estimate the ocean interior state and the TC radius of maximum winds. Such a diagnostic thus explains the dominant baroclinic ocean response to a TC passage, and, inversely, can be used to infer ocean stratification or forcing parameters in the absence of high-resolution observations.

1. Introduction

Cold wakes are marked distinctive footprints of the air-sea interactions occurring during the passages of moving Tropical Cyclones (TCs), with intense near-inertial waves (NIWs) dispersing through the ocean column (Geisler, 1970; Gill, 1984; Shay & Elsberry, 1987). Strong shear currents at the base of the mixed layer (ML) (Gill, 1984; E. A. D'Asaro, 1985) can reach 1–3 $m.s^{-1}$, penetrate deeply into the thermocline (Firing, 1997), to erode the initial stratification, leaving quite systematically persisting sea surface anomalies, that is, cooling (Price, 1981), chlorophyll bloom (I. Lin et al., 2003; Babin et al., 2004; Walker et al., 2014) and salinity rise (Girishkumar et al., 2014; Reul et al., 2014). At depth, isopycn displacements leave thermocline ridges (Geisler, 1970) that strengthen the injection of subsurface anomalies (Brizuela et al., 2023), leading to measurable sea level depressions (Geisler, 1970; Ginis & Sutyrin, 1995; Shay et al., 1989). Both barotropic (column-integrated current) and baroclinic modes participate to sea surface height anomalies (SSHA), but the latter is largely dominant for open ocean conditions (Ginis & Sutyrin, 1995).

Sea surface temperature anomalies (SSTA) have extensively been documented (Fisher, 1958; Leipper, 1967; Price, 1981; Stramma et al., 1986; Park et al., 2011; Vincent et al., 2012; Mei et al., 2015; S. Lin et al., 2017). More recent, sea surface salinity anomalies (SSSA) are now reported from L-band micro-wave satellite sensors (Reul et al., 2021; Sun et al., 2021) and interior ocean Argo profiles (Reul et al., 2014). Detailing the wake current system has been performed for specific cases with current profilers (Sanford et al., 1987; Sanford et al., 2011; Price et al., 1994; E. A. D'Asaro et al., 2007; Black et al., 2007) or moored measurements (Brink, 1989;

Visualization: Clément Combot, Alexis Mouche, Bertrand Chapron
Writing – original draft: Clément Combot, Alexis Mouche, Bertrand Chapron
Writing – review & editing: Clément Combot, Alexis Mouche, Bertrand Chapron

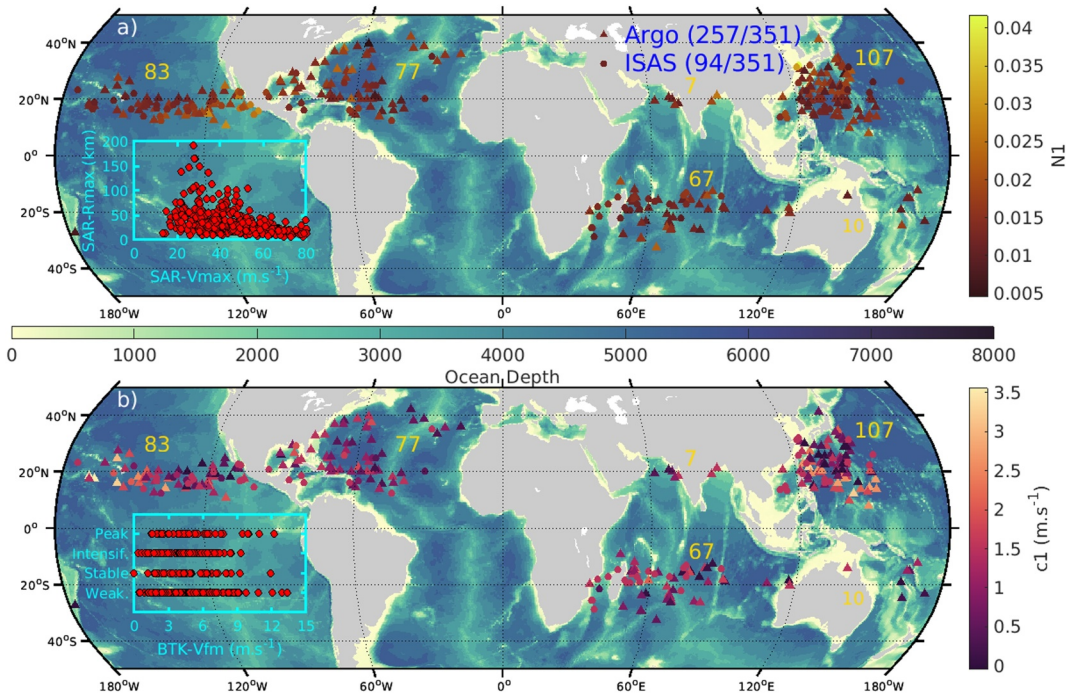

Figure 1. Global distribution of TCs center positions from SAR acquisitions across tropical basins for 2015–2022 time period, according to co-location situation with in-situ measurements (triangle, when Argo float existing; circle, when ISAS is used instead), and stratification parameters: (a) the averaged brunt-Väisälä frequency of the seasonal Thermocline, (b) the phase speed of the first baroclinic mode. Ocean depth is represented as the background for both panels. The SAR sampling is indicated for each cyclonic basin, as well as the distribution of TC properties through two embedded graphs.

Brooks, 1983; Shay & Elsberry, 1987). Sea surface height anomalies (SSHA) remain somehow overlooked. Kudryavtsev, Monzikova, Combot, Chapron, Reul, et al. (2019) developed a semi-empirical framework to relate the main atmospheric forcing and ocean interior parameters to the TC wake probed by altimeters. Yet, their reported analysis was restricted to a short number of cases, and used reanalysis products as ancillary information.

Following the multi-modal strategy of the CBLAST experiment in North Atlantic (Black et al., 2007; Sanford et al., 2011) or ITOP program in south China Sea (Pun et al., 2011; E. D'Asaro et al., 2011; E. A. D'Asaro et al., 2014), we built an extensive database, to extend this logic to a global scale (see Figure 1). It mostly relies on the capabilities of L2/L3 microwave (MW) satellite measurements and the now growing collection of Argo profilers. Previous studies separately proved the efficiency of the existing networks to infer TC forcing information from Synthetic Aperture Radar high-resolution observations (A. Mouche et al., 2019; Combot, Mouche, et al., 2020), to the ocean responses with altimeters/radiometers (Kudryavtsev, Monzikova, Combot, Chapron, Reul, et al., 2019; Reul et al., 2014) and the ocean stratification with Argo (Reul et al., 2014). Section 2 presents the methodology relative to each instrument of our database. Combined estimates allow both a comprehensive SSHA analysis and a better monitoring of TC cold wake parameters (Combot, Quilfen, et al., 2020). Section 3 presents results of the semi-empirical law of baroclinic responses at global scale. Section 4 further analyzes SSHA signals relative to the estimated forcing terms. Main results are recalled Section 5, highlighting the significant contribution of highly resolved observations to interpret the upper ocean responses.

2. Methodology

Our approach is based on a novel combination of highly resolved spaceborne and in-situ observations. This is central to our multi-modal strategy to investigate atmospheric forcing, ocean stratification and the associated sea surface response. Figure 1 shows the overall extent of the database. The analysis is constrained by SAR acquisitions (represented by markers). SAR measurements provides unique information but has a more limited temporal resolution than the other MW observations presented here. Each measurement and the associated extraction

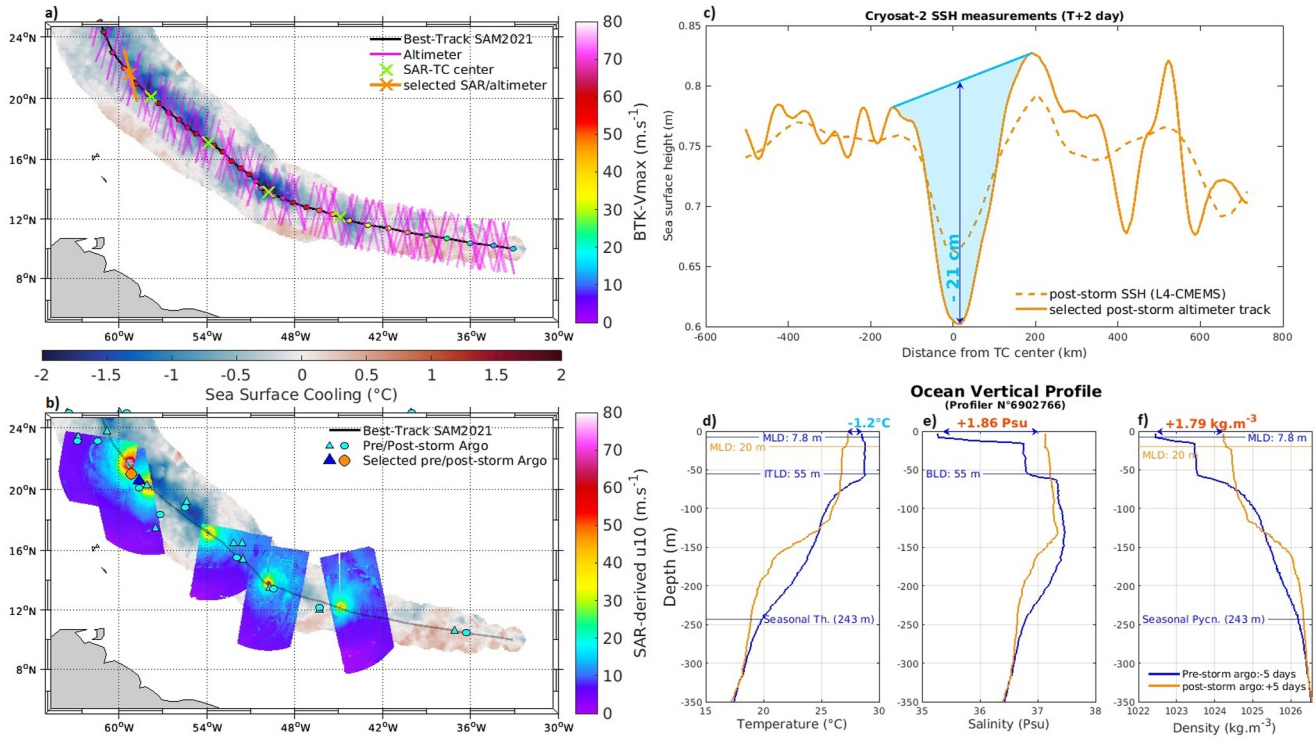

Figure 2. Illustration of the multimodal analysis of the cold wake of hurricane Sam, with (a) the altimeter coverage along the track (with in color V_{max} from BTK) and the positions of TC center from SAR sampling. The corresponding swaths are shown in panel (b) with the Argo floats collected within the maximum extent of r34 at each synoptic times. Two illustrative measurements, located at the positions of the orange markers in (a) and (b), are displayed: with (c) the post-storm SSH measurements from Cryosat-2 and the associated estimates of the L4-CMEMS daily product interpolated along the altimeter track, and the Pre- and Post-storm ocean vertical profiles of (d) temperature, (e) salinity and (f) density from Argo within Sam cold wake. MLD: mixed layer depth, ITLD: isothermal layer depth, BLD: Barrier layer depth. SSTA are also shown in (a) and (b) in shaded colors.

method are illustrated in Figure 2, with the specific example of Hurricane Sam, a major hurricane with distinctive response that occurred in 2021.

2.1. Atmospheric Forcing: SAR and BTK

Cyclonic forcing can be reduced to the combination of three main parameters: the maximum wind speed, V_{max}, its radius of action, R_{max}, and the TC translation speed, V_{fm} (forward motion) which reflects the coupling time (Lloyd & Vecchi, 2011). Here they are provided by SAR measurements or Best-track (BTK) analysis.

One of the largest SAR database for TC analysis is constituted of 351 images, acquired between 2015 and 2022 by C-band SARs from Sentinel-1 constellation (two satellite units S1a and S1b Supporting Information S1) operated by Copernicus/European Space Agency (A. A. Mouche et al., 2017) and from Radarsat-2 sensor of the Canadian Space Agency program (Banal et al., 2007). In contrast to other low-orbit satellite platforms, SAR missions cannot perform continuous acquisitions and have different exclusive acquisition modes. This implies the development of specific strategies to monitor TC (A. Mouche et al., 2019). Both missions benefit dual-polarization measurements (VV + VH/HH + HV), essential to provide fine-scale TC inner core wind estimates, with an effective resolution of about 1 km over a wide swath ranging from 250 to 500 km, depending on the instrument and acquisition mode used (A. A. Mouche et al., 2017). The wind retrieval algorithm combined co- and cross-polarized radar signals (A. A. Mouche et al., 2017; A. Mouche et al., 2019), that was proved to fully capture both V_{max}/R_{max} variabilities, compared to concomitant SFMR measurements (Combot, Mouche, et al., 2020). These inner core parameters are extracted from each SAR scene (Figure 2b) by strictly following the methodology developed in Combot, Mouche, et al. (2020), with a progressive wind transect decomposition method (see Supporting Information S1 for further details). For each acquisition, we also derived the maximum extent of the radius of 17 $m.s^{-1}$ (r17), which is a good metric of the overall storm size (in general, radii from r17 to

r12, Holland and Merrill (1984); K. T. F. Chan and Chan (2012); K. T. Chan and Chan (2015); J. Zhang et al. (2019)) and will later be used to define the area for in-situ data collection.

TC centers extracted from SAR images (markers in Figure 1, crosses in Figure 2a) are then used to gather all other observations; the space-time frame is determined from the adjacent positions given by the Best-track (Figure 2a), which provides post-storm analyses of TC vitals and positions at each synoptic time (every 6h, like V_{max} in Figures 2a and 2b), carried out by several official centers across tropical basins (Knapp et al., 2010, 2018). For the sake of consistency, we only refer to information documented by National Hurricane Center (NHC) for AT and EP, or by the Joint Typhoon Warning Center (JTWC) for the other basins, both using similar conventions (1-min maximum sustained winds) and data assimilation system (Knaff et al., 2021; Sampson & Schrader, 2000). From best-track successive positions, the translation speed is estimated, along interpolated size and intensity parameters at the time of the SAR image, that will be also used as source of comparison.

2.2. Ocean Stratification: Argo and ISAS

At ocean level, vertical stratification further modulates the wake amplitude (Shay, 2009). The bulk of the oceanic response is contained in the first baroclinic modes (Ginis & Sutyrin, 1995). We focus on the Seasonal Thermocline (STh), where the temperature gradient is the greatest (see Figure 2d), to derive an average Brunt-Väisälä frequency(N_1) (More details are provided in the Supporting Information S1).

The maximum extent (r17) is used to collect free-drifting profiling Argo floats associated with each SAR scene (see Figure 2b), within a temporal window of 15 days prior to the storm. Argo floats document the vertical profile of temperature and salinity over a depth of 2000 m, within a 10-day cycle (Freeland et al., 2010), with a great accuracy (±0.002°C and 2.4 dbar Wong et al. (2020)) after some delayed-mode adjustments conducted by the Global Data Assembly Centers (GDACs). With more than 4,000 units (Roemmich et al., 2009, 2019), the Argo network provides significant coverage of the ocean stratification in tropical basins. Over 70% of the TC cases considering in this study benefits from Argo (see Figure 1). As for hurricane Sam, the available floats are represented along the track and meet the collocation criteria for four of the five SAR acquisitions (Figure 2b).

Each vertical profile collected is then broken down into a three-layer ocean interior, following Kudryavtsev, Monzikova, Combot, Chapron, Reul, et al. (2019) to isolate the STh. The profile, closest in time and space, is used to define the stratification prior to the storm passage. The mixed layer depth (MLD) is also evaluated, using the 0.2°C robust criterion (de Boyer Montégut et al., 2004). The MLD along with the STh depth (see Figures 2d and 2f), is used to characterize the phase speed of the first baroclinic mode, c1, to define a Froude number (see definition in Supporting Information S1), a metric helping to identify the regime of the ocean response. Both c1 and N1 values are displayed in panel a and b of Figure 1, with a stronger variability in the North Pacific basins.

In the absence of in-situ data (30% of the global data set), the climatological product ISAS-15 is used to derive N1 (Gaillard et al., 2016).

2.3. Ocean Response: Sea Surface Anomalies

Finally, altimeters and radiometers are used to retrieve respectively TC wake SSH and SST anomalies.

The altimeter constellation has grown from 3/4 instruments at the start of the 2010 decade to 6/8 instruments for our sample period (2015–2022 (Abdalla et al., 2021),), providing unprecedented coverage of dynamic ocean topography, for example, Figure 2a. To recall, only altimeter tracks co-located with the SAR detected TC centers are kept, within two adjacent BTK points. The sampling period spans a window of 1–7 days after the TC, with the response generally peaking between 1 and 4 inertial periods (in tropical region 1 IP = 24–40hr). Along-track altimeters provide SSH estimates every 7 km resolution, as distributed by the Copernicus service (CMEMS). These measurements generally allow to catch the TC surface trough (SSHA), although not completely resolving the inertial patterns.

Due to the prominence of the TC-induced signature, SSHA can directly be estimated from the sole use of post-storm altimeter measurements, Figure 2c with a 21 cm estimated depression. This method provides an unique description of the air/sea interactions occurring during a TC passage. No pre-storm mean conditions derived from L4-product are used, to avoid smoothing effects inherent to these products, for example, Figure 2c illustrating a drastic softening signature of the daily product interpolated in time and space along the Cryosat-2 track.

TC SAM cold wake is derived from the REMSS product, using a strategy presented by Reul et al. (2014). In some cases, Figure 2b, pair of Argo floats may be also present, making it possible to probe the vertical profiles before and after the TC. Here, a modest temperature response (1.2°C) is observed (Figure 2d), in agreement with satellite data, accompanied by a strong salinity wake (Figure 2e). More dedicated analysis of SSTA will be the subject of a future study.

2.4. Methodology Outcomes

These combined observations leads to the extraction of one synthetic wake variable (SSHA) and four initial parameters: two describing the cyclonic forcing ($V_{\max}$, $R_{\max}$), an environmental factor for the ocean interior (N1) and one for the coupling (V_{fm}). A number of ambiguous signatures were removed, when data were deemed too erratic (island, coastal cases: 45 cases) or the situations too complex (global current regime, too weak signatures from tropical depression: 36 cases). Ultimately, 270 cases among the database have been kept (for which 80% covered by Argo), providing a wide range of forcing conditions (Figure 1a), stratification (Figure 1a) and wake signatures.

3. The Baroclinic Response Scaling Law

The modulation of the wake response (hereafter $\delta\eta$ = SSHA) can be quantified by a simple semi-empirical law, combining the four extracted parameters (see Kudryavtsev, Monzikova, Combot, Chapron, Reul, et al. (2019) for details):

$$g.\delta\eta/V_{\max}^2 \propto R_{\max}N_1/V_{fm} \quad (1)$$

It corresponds to a simplification of the three-dimensional inertial wake problem, described by the full analytical solution (Kudryavtsev, Monzikova, Combot, Chapron, & Reul, 2019), which combines both baroclinic and barotropic responses in a three-layers model. Several simplifying assumptions lead to this scaling law. (a) Since the coupling between the two response modes is weak, both modes are treated independently (Geisler, 1970). (b) The baroclinic response is dominant in open ocean (Ginis & Sutyrin, 1995), and Equation 1 solely synthetizes its dynamic. (c) The ocean modulation is mostly driven by the seasonal thermocline stratification (i.e., the mixed layer is transparent). The sea surface trough is merely an integration of changes associated to internal displacements of the seasonal thermocline (Kudryavtsev, Monzikova, Combot, Chapron, Reul, et al., 2019). (d) The surface response is strongly related to the TC size and forcing stress, proportional to $R_{\max}{*}V_{\max}{}^2$. (e) At last, this empirical relationship comes from a linearization of the momentum balance. Advection term is removed, and the resulting scaling law mostly translates the dominant contribution of the wind-induced turbulent mixing (Price, 1981).

Figure 3 graphically confirms the validity of this baroclinic scaling law, already verified for few TC cases in the eastern Pacific (Combot, Quilfen, et al., 2020; Kudryavtsev, Monzikova, Combot, Chapron, Reul, et al., 2019), now, extrapolated to all basins and to a much larger data set. Its robustness is also underlined by strong correlations observed (>0.7), irrespective of the forcing used. The correlation using BTK forcing (0.73, left column) is similar to the one previously reported (0.79 in Kudryavtsev, Monzikova, Combot, Chapron, Reul, et al. (2019)), demonstrating the consistency of these results despite methodological differences. The scaling law performance markedly improves when high-resolution SAR measurements are used (right column), with a very high correlation of 0.862 and a clear reduction in data dispersion.

Some outliers can be noticed, corresponding to responses dominated by the barotropic component, outside the scope of the scaling law validity. Three criteria are used to filter these limiting cases: a) an ocean depth H < 2000 m (Jansen et al., 2010), a Froude number less than 1 (Geisler, 1970) or a low dimensionless translation speed (E. A. D'Asaro et al., 2014; Reul et al., 2021) S < 0.5 (see definition in Supporting Information S1). These criteria determine respectively, whether the barotropic response will be strongly amplified by a shallow water column (Jansen et al., 2010), or whether the cyclone energy is transferred to the surface barotropic circulation rather than the inertial one (Ginis, 2002)- or by a cyclone sufficiently stationary to allow efficient Ekman pumping, which compromises the linear response assumption of the model (Jullien et al., 2012). At last 49 cases are identified, reducing the data set to 221 cases (still ~80% covered by Argo).

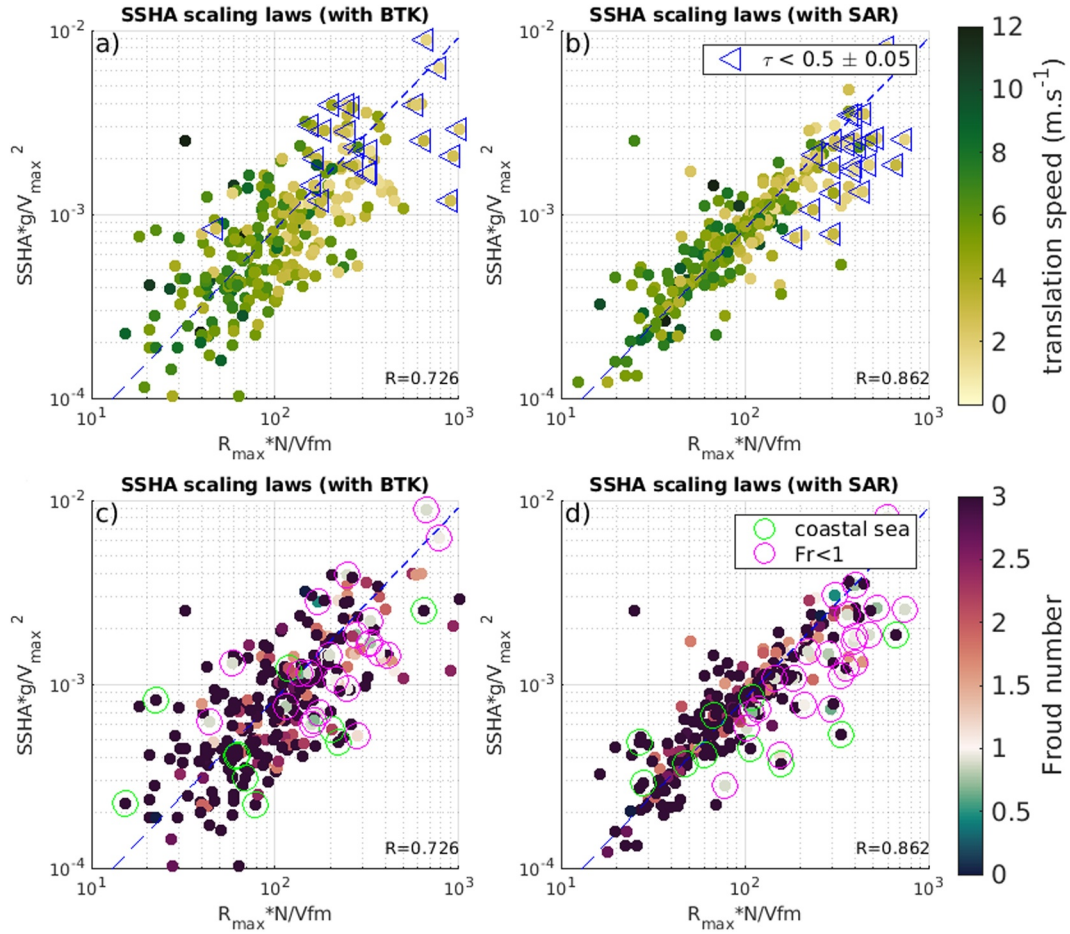

Figure 3. Scaling of the TCs-induced SSHA documented by Best-Track forcing (V_{max}/R_{max}), panels (a) and (c); and by SAR measurements, panels (b) and (d), with indications of translation speed (upper panels), or Froude number (lower panels). Marginal situations corresponding to the development of a barotropic-like response are indicated by pink circles for sub-critical translation speeds, by blue triangles for small adimensional storm speed, and by green circles for cases in coastal environments (H<2000 m).

From this scaling law, regression coefficients can be calculated to directly predict SSHA from the initial parameters. Results are similar to those previously provided (Kudryavtsev, Monzikova, Combot, Chapron, Reul, et al., 2019):

$$\delta\eta = 6.9.10^{-6}\left(V_{\max}^2/g\right)\left(R_{\max}N_1/V_{fm}\right)^{1.041} \quad (2)$$

4. Analysis of the SSHA Distribution and Trend

The inverse law provides a direct diagnosis of ocean responses induced by TCs, Figure 4a. The combination of high-resolution observations for forcing parameters and ocean stratification provides extremely reliable estimates of SSHA, with a significant and almost unbiased correlation of 0.94. The median deviation of 1.56 cm from altimetry measurements is particularly small and of the order of the instrumental biases (Abdalla et al., 2021). Consequently, the modulation of the different parameters is correctly interpreted by the model, and associated variations are well taken into account by the in-situ and satellite observations. A mild scattering is observed (22%), with the presence of a few erratic values that slightly increase the RMSE to 3.4 cm, although their implication remains modest given its proximity to the median value. These more ambiguous estimates may correspond to cases contaminated by rain (erroneous V_{max} (Combot, Mouche, et al., 2020),), to a smaller altimeter sampling (underestimation of SSHA), or even to situations with a deep dual-mode response (i.e., barotropic/baroclinic) for the strongest estimates (around 0.4 m).

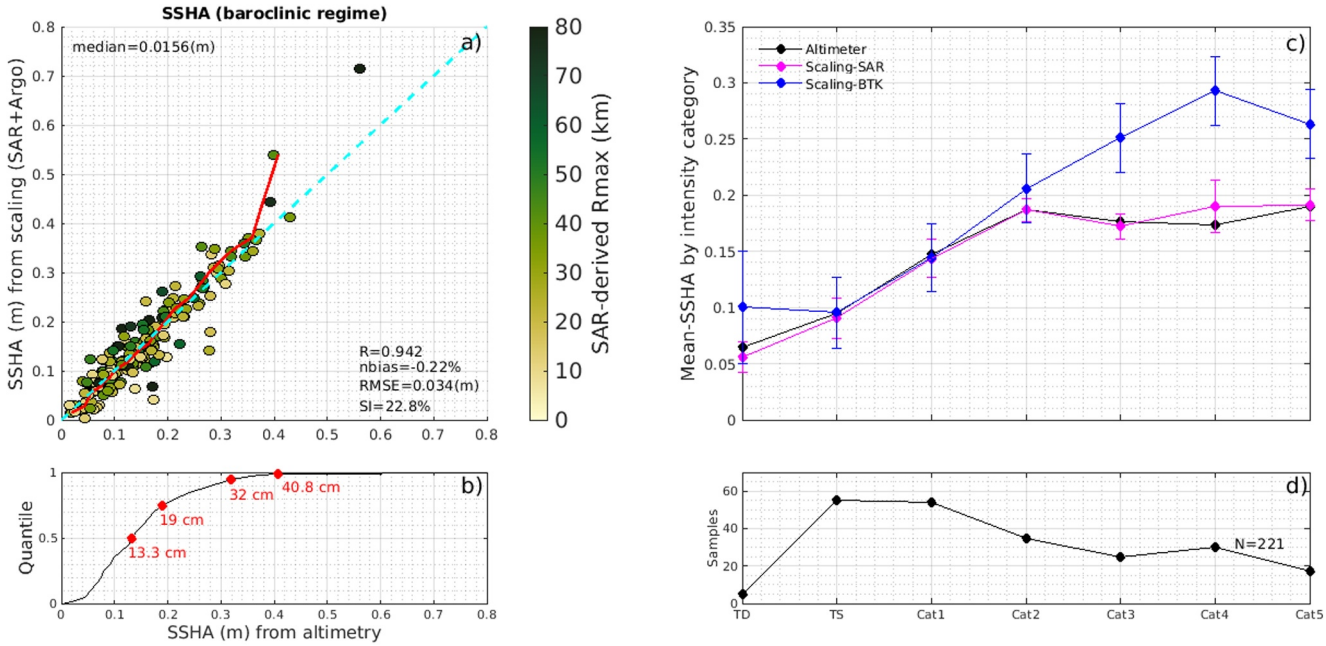

Figure 4. Analysis of the baroclinic response, with (a) the comparison between the SSHA measured from altimeters and the ones estimated from the inversion of the scaling law documented by SAR and Argo, and (c) the averaged-trend of the mean SSHA according to wind intensity category, for SAR-derived (magenta) and BTK-derived scaling retrieval (blue) and for observations (black), vertical bars indicate the standard deviations. The two lower panels disclose statistics properties of the analysis, the quantile distribution of the SSHA amplitudes observed for (b), and the sampling according to each wind intensity category for (d).

The quantile-quantile curve shows excellent congruence between the distribution of observed and predicted values along the interval [0 0.4]m, until responses about 40 cm, which encompass intermediate cases with a Froude number or dimensionless translation speed close to critical values. The strongest amplitudes can be observed for some barotropic situations, with SSHA around 80 cm. Figure 4b displays more restrictive distribution of baroclinic wakes from 0 to 40 cm, with values mainly concentrated around 10–20 cm (50%), which enfolds most of cyclonic activity (>=Cat 1). About 30% of troughs are below 10 cm and mostly correspond to tiny or weak systems like TD, 20% are above 20 cm and correspond to intense/slow or intense/large systems. Baroclinic responses around 40 cm are therefore very rare (<1%), the 50th percentile being 13.3 cm, as weak systems like tropical storms account for a significant proportion of the total activity (25% of the data set, Figure 4d).

Figure 4c further sheds light on the non-monotonic relationship between surface anomalies and intensity (averaged by category, see sampling in Figure 4d). Besides excellent agreement between the altimeter measurements and scaling law predictions, an asymptotic trend is seemingly emerging for major systems (>=Cat3), echoing similar evolutions of SSTA reported by Reul et al. (2014) and Mei et al. (2015). This trend is poorly anticipated when BTK forcing is used, and a significant divergence appears for stronger categories. These discrepancies mostly stem from R_{max} reported by BTK, which overestimate the inner core size for intense systems (Combot, Mouche, et al., 2020). Major systems tend (on average) to have a smaller R_{max}, which compensates for the effects of intensity to limit wake amplitudes, yet this decrease in R_{max} is generally not taken into account by BTK for small systems and tends to follow an asymptotic behavior due to the coarse resolution of the observations used.

5. Discussion and Conclusion

The results show that, reduced to the SSHA, the three-dimensional ocean response to TC passages can be robustly synthesized through a mean response of the seasonal thermocline (N_1) to a moving (V_{fm}) cyclonic forcing $\left(R_{max}V_{max}^2\right)$. Using an innovative observation-based method, the baroclinic nature of the TC cold wake observed in open ocean is confirmed (Geisler, 1970; Ginis & Sutyrin, 1995; Kudryavtsev, Monzikova, Combot, Chapron, Reul, et al., 2019). Identified barotropic responses were filtered out. However, good congruence was

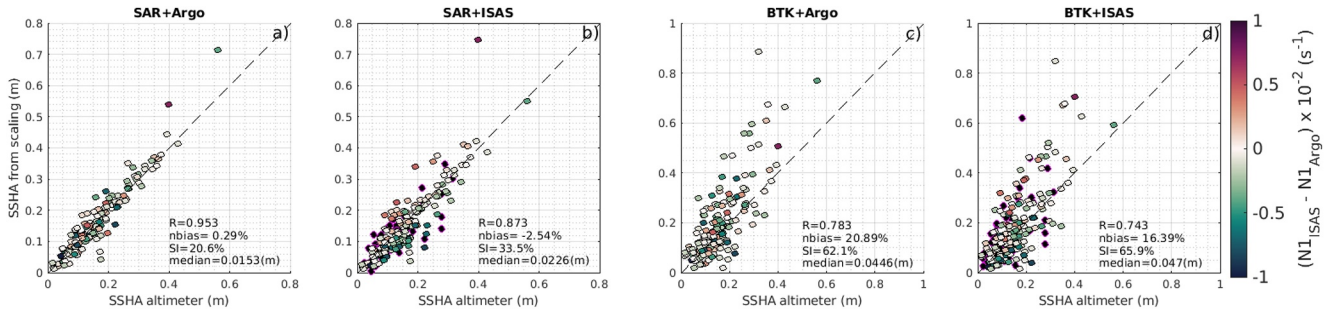

Figure 5. Evolution of the quality of SSHA predictions when derived from (a) SAR and Argo measurements, (b) SAR and ISAS climatology, (c) BTK and Argo and (d) BTK and ISAS. The colorbar indicates the discrepancies of stratification between the climatology estimates and in-situ measurements:($N1_{ISAS} - N1_{Argo}$). The black dots with a magenta outline represent situations where we have no Argo data and where stratification depends solely on ISAS climatology (54 cases).

still observed, validating the semi-empirical scheme and hypothesis of Kudryavtsev, Monzikova, Combot, Chapron, Reul, et al. (2019). The use of a semi-empirical law for the baroclinic response, combined with a multi-modal database, provides an almost complete interpretation of the mean TC wake response, to anticipate most of the amplitudes of surface troughs, about 63% of total cases (221/351), in line with previous studies (∼70% in Jullien et al. (2012); H. Zhang et al. (2020)). In addition, an asymptotic behavior is revealed with respect to TC intensity, and most baroclinic signatures range from 0 to 40 cm, with an average sea level depression about 10–20 cm.

If both atmospheric forcing sources provide good correlation (at least ∼0.7), when in situ measurements of stratification are combined with highly resolved atmospheric forcing observations, results significantly improve. Figure 5 summarizes the substantial contribution of these measurements to the accuracy of SSHA estimates, with progressive declines in all statistical indicators when SAR and Argo data are successively removed from the analysis (from R = 0.95 to r = 0.74, Figure 5a). Overall, forcing parameters have a greater weight to interpret the ocean response (Figures 5a and 5c), which confirms the very strong dependence of SSHA on atmosphere momentum fluxes. An accurate definition of TC inner core is required to correctly integrate the effects of stratification, as suggested with the more ambiguous discrepancies between the BTK + Argo and BTK + ISAS solutions (Figures 5c and 5d). While the in-situ data seem to often be in line with the climatology, significant discrepancies can still occur and radically compromise the analysis when ISAS parameters are used (Figure 5b).

Using high-resolution data may seem restrictive due to the scarcity of SAR and in situ observations. But, with the present-day altimeter constellation, the semi-empirical law provides an efficient and versatile method to diagnose air/sea interactions during a TC. It can help not only to investigate wake amplitudes but also to revisit other coupling parameters, such as $R_{\max}$ or even stratification. This limited spatio-temporal sampling shall also improve in the future, with the advent of Radarsat constellation mission (RCM) launched in 2019 (Geldsetzer et al., 2019; Kroupnik et al., 2021; Séguin & Ahmed, 2009), future European L-band sensor (ROSE-L, Davidson and Furnell (2021); Moreira et al. (2023); Perna et al. (2024)), and foreseen EE 10 Harmony mission (López-Dekker et al., 2021), that will gradually enrich the capability to monitor the surface wind structure at very high resolution under extreme conditions. It is also worth mentioning the emergence of new altimeter capabilities with the SWOT instrument, which will provide unique 2D maps of TC wakes. This will ease the proposed analysis and the automation of the proposed SSHA extraction method, to make these results more reproducible. This expanded constellation of SAR and altimeters missions shall considerably enrich our database to further investigate the coupling mechanisms between the TC vortex and the ocean interior.

Finally, TC Sam inertial response was strong with a trough larger than 20 cm, but the temperature response was seemingly relatively small (around 1°C, see also Figure S3 from Supporting Information S1) unlike the salinity signature. Surface mixing was likely partially inhibited due to the existence of a barrier layer, noticeable in the Argo profiles (Figures 2d and 2e). A next investigation will explore the differences between surface and subsurface dynamics occurring in TC cold wakes.

Data Availability Statement

Ocean vertical profiles from Argo are collected by GDACS and are distributed by Ifremer: https://data-argo.ifremer.fr/geo. High-resolution winds derived from the combination of cross- and co-polarized SAR signal are retrieved and provided by Ifremer: https://data-maxss.ifremer.fr (see *added_value/tc − vortex − radii*). Daily satellite-based SST product from REMSS can be found at https://data.remss.com/sst/daily/mw_ir/v05.0/netcdf. L3 measurements of SSH for each altimeter were provided by CMEMS (2024). Best-track parameters are provided by IBTrACS on: https://www.ncei.noaa.gov/products/international-best-track-archive (Gahtan et al., 2024).

Acknowledgments
The authors would like to thank Yves Quilfen for his co-supervision and significant contribution to this work, with his seminal study on tracking SSHA in the wake of TCs, using under-track altimeter observations. This work is part of the ESA Marine Atmosphere eXtreme Satellite Synergy project (MAXSS) https://www.maxss.org/science.

References

Abdalla, S., Abdeh Kolahchi, A., Ablain, M., Adusumilli, S., Aich Bhowmick, S., Alou-Font, E., et al. (2021). Altimetry for the future: Building on 25 years of progress. *Advances in Space Research*, *68*(2), 319–363. https://doi.org/10.1016/j.asr.2021.01.022

Babin, S. M., Carton, J. A., Dickey, T. D., & Wiggert, J. D. (2004). Satellite evidence of hurricane-induced phytoplankton blooms in an oceanic desert. *Journal of Geophysical Research*, *109*(3), 1–21. https://doi.org/10.1029/2003jc001938

Banal, S., Iris, S., & Saint-Jean, R. (2007). Canadian space agency's hurricane watch program: Archive contents, data access and improved planning strategies. In *2007 ieee international geoscience and remote sensing symposium* (pp. 3494–3497). IEEE. https://doi.org/10.1109/IGARSS.2007.4423599

Black, P. G., D'Asaro, E. A., Drennan, W. M., French, J. R., Niiler, P. P., Sanford, T. B., et al. (2007). Air-sea exchange in hurricanes. *Bulletin America Meteorology Social*, *88*(3), 357–374. https://doi.org/10.1175/bams-88-3-357

Brink, K. H. (1989). Observations of the response of thermocline currents to a hurricane. *Journal of Physical Oceanography*, *19*(7), 1017–1022. https://doi.org/10.1175/1520-0485(1989)019⟨1017:OOTROT⟩2.0.CO;2

Brizuela, N. G., Alford, M. H., Xie, S. P., Sprintall, J., Voet, G., Warner, S. J., et al. (2023). Prolonged thermocline warming by near-inertial internal waves in the wakes of tropical cyclones. *Proceedings of the National Academy of Sciences of the United States of America*, *120*(26), 1–9. https://doi.org/10.1073/pnas.2301664120

Brooks, D. A. (1983). The wake of hurricane allen in the western Gulf of Mexico. *Journal of Physical Oceanography*, *13*(1), 117–129. https://doi.org/10.1175/1520-0485(1983)013⟨0117:TWOHAI⟩2.0.CO;2

Chan, K. T., & Chan, J. C. (2015). Impacts of vortex intensity and outer winds on tropical cyclone size. *Quarterly Journal of the Royal Meteorological Society*, *141*(687), 525–537. https://doi.org/10.1002/qj.2374

Chan, K. T. F., & Chan, J. C. L. (2012). Size and strength of tropical cyclones as inferred from QuikSCAT data. *Monthly Weather Review*, *140*(3), 811–824. https://doi.org/10.1175/MWR-D-10-05062.1

CMEMS. (2024). Global ocean along track l3 sea surface heights reprocessed 1993 ongoing tailored for data assimilation. [dataset]. *e.u. copernicus marine service information (cmems). marine data store (mds)*. https://doi.org/10.48670/MOI-00146

Combot, C., Mouche, A., Knaff, J., Zhao, Y., Zhao, Y., Vinour, L., et al. (2020). Extensive high-resolution synthetic aperture radar (SAR) data analysis of tropical cyclones: Comparisons with SFMR flights and best-track. *Monthly Weather Review*, *148*(11), 1–67. https://doi.org/10.1175/MWR-D-20-0005.1

Combot, C., Quilfen, Y., Mouche, A., Gourrion, J., de Boyer Montégut, C., Chapron, B., & Tournadre, J. (2020). Space-based observations of surface signatures in the wake of the 2018 Eastern Pacific tropical cyclones. *Journal of Operational Oceanography*, *13*(sup1), S132–S137. https://doi.org/10.1080/1755876X.2020.1785097

D'Asaro, E., Black, P., Centurioni, L., Harr, P., Jayne, S., Lin, I., et al. (2011). Typhoon-Ocean interaction in the western North Pacific: Part 1. *Oceanography*, *24*(4), 24–31. https://doi.org/10.5670/oceanog.2011.91

D'Asaro, E. A. (1985). The energy flux from the wind to near-inertial motions in the surface mixed layer. *Journal of Physical Oceanography*, *15*(8), 1043–1059. https://doi.org/10.1175/1520-0485(1985)015⟨1043:TEFFTW⟩2.0.CO;2

D'Asaro, E. A., Black, P. G., Centurioni, L. R., Chang, Y. T., Chen, S. S., Foster, R. C., et al. (2014). Impact of typhoons on the ocean in the pacific. *Bulletin of the American Meteorological Society*, *95*(9), 1405–1418. https://doi.org/10.1175/BAMS-D-12-00104.1

D'Asaro, E. A., Sanford, T. B., Niiler, P. P., & Terrill, E. J. (2007). Cold wake of hurricane frances. *Geophysical Research Letters*, *34*(15), 2–7. https://doi.org/10.1029/2007GL030160

Davidson, M. W. J., & Furnell, R. (2021). ROSE-L: Copernicus L-band sar mission. In *2021 ieee international geoscience and remote sensing symposium igarss* (pp. 872–873). IEEE. https://doi.org/10.1109/IGARSS47720.2021.9554018

de Boyer Montégut, C., Madec, G., Fischer, A. S., Lazar, A., & Iudicone, D. (2004). Mixed layer depth over the global ocean: An examination of profile data and a profile-based climatology. *Journal of Geophysical Research C: Oceans*, *109*(12), 1–20. https://doi.org/10.1029/2004JC002378

Firing, E., Lien, R., & Muller, P. (1997). Observations of strong inertial oscillations after the passage of Tropical Cyclone Ofa. *Journal of Geophysical Research C: Oceans*, *102*(C2), 3317–3322. https://doi.org/10.1029/96JC03497

Fisher, E. L. (1958). Hurricanes and the sea-surface temperature field. *Journal of Meteorology*, *15*(3), 328–333. https://doi.org/10.1175/1520-0469(1958)015⟨0328:hatsst⟩2.0.co;2

Freeland, H. J., Freeland, H. J., Freeland, H. J., Freeland, H. J., Freeland, H. J., & Freeland, H. J. (2010). Argo - a decade of progress. In *Proceedings of oceanobs'09: Sustained ocean observations and information for society* (Vol. 44, pp. 332–345). European Space Agency. https://doi.org/10.5270/OceanObs09.cwp.32

Gahtan, J., Knapp, K. R., Schreck, C. J. I., Diamond, H. J., Kossin, J. P., & Kruk, M. C. (2024). International best track archive for climate stewardship (ibtracs) project, version 4.01, csv data. NOAA National Centers for Environmental Information. [dataset]. https://doi.org/10.25921/82ty-9e16

Gaillard, F., Reynaud, T., Thierry, V., Kolodziejczyk, N., & Von Schuckmann, K. (2016). In situ-based reanalysis of the global ocean temperature and salinity with ISAS: Variability of the heat content and steric height. *Journal of Climate*, *29*(4), 1305–1323. https://doi.org/10.1175/JCLI-D-15-0028.1

Geisler, J. E. (1970). Linear theory of the response of a two layer ocean to a moving hurricane. *Geophysical Fluid Dynamics*, *1*(1–2), 249–272. https://doi.org/10.1080/03091927009365774

Geldsetzer, T., Khurshid, S. K., Warner, K., Botelho, F., & Flett, D. (2019). Wind speed retrieval from simulated radarsat constellation mission compact polarimetry sar data for marine application. *Remote Sensing*, *11*(14), 1682. https://doi.org/10.3390/rs11141682

Gill, A. E. (1984). On the behavior of internal waves in the wakes of storms. *Journal of Physical Oceanography*, *14*(7), 1129–1151. https://doi.org/10.1175/1520-0485(1984)014⟨1129:OTBOIW⟩2.0.CO;2

Ginis, I. (2002). Tropical cyclone-ocean interactions. In *Advances in fluid mechanics* (pp. 83–114).

Ginis, I., & Sutyrin, G. (1995). Hurricane-generated depth-averaged currents and sea surface elevation. *Journal of Physical Oceanography*, *25*(6), 1218–1242. https://doi.org/10.1175/1520-0485(1995)025⟨1218:HGDACA⟩2.0.CO;2

Girishkumar, M. S., Suprit, K., Chiranjivi, J., Udaya Bhaskar, T. V., Ravichandran, M., Shesu, R. V., & Pattabhi Rama Rao, E. (2014). Observed oceanic response to tropical cyclone Jal from a moored buoy in the south-western Bay of Bengal. *Ocean Dynamics*, *64*(3), 325–335. https://doi.org/10.1007/s10236-014-0689-6

Holland, G. J., & Merrill, R. T. (1984). On the dynamics of tropical cyclone structural changes. *Quarterly Journal of the Royal Meteorological Society*, *110*(465), 723–745. https://doi.org/10.1002/qj.49711046510

Jansen, M. F., Ferrari, R., & Mooring, T. A. (2010). Seasonal versus permanent thermocline warming by tropical cyclones. *Geophysical Research Letters*, *37*(3). https://doi.org/10.1029/2009GL041808

Jullien, S., Menkes, C. E., Marchesiello, P., Jourdain, N. C., Lengaigne, M., Koch-larrouy, A., et al. (2012). Impact of tropical cyclones on the heat budget of the South Pacific Ocean. *Journal of Physical Oceanography*, *42*(11), 1882–1906. https://doi.org/10.1175/JPO-D-11-0133.1

Knaff, J. A., Sampson, C. R., Kucas, M., Slocum, C. J., Brennan, M. J., Meissner, T., et al. (2021). Estimating tropical cyclone surface winds: Current status, emerging technologies, historical evolution, and a look to the future. *Tropical Cyclone Research and Review*, *10*(3), 125–150. https://doi.org/10.1016/j.tcrr.2021.09.002

Knapp, K. R., Diamond, H. J., Kossin, J. P., Kruk, M. C., & Schreck, C. J. (2018). International best track archive for climate stewardship (IBTrACS) project, version 4. *(Tech. Rep.)*. https://doi.org/10.25921/82ty-9e16

Knapp, K. R., Kruk, M. C., Levinson, D. H., Diamond, H. J., & Neumann, C. J. (2010). The international best track archive for climate stewardship (IBTrACS). *Bulletin of the American Meteorological Society*, *91*(3), 363–376. https://doi.org/10.1175/2009BAMS2755.1

Kroupnik, G., De Lisle, D., Cote, S., Lapointe, M., Casgrain, C., & Fortier, R. (2021). RADARSAT constellation mission overview and status. In *IEEE national radar conference - proceedings, 2021-may(march)* (pp. 1–5). https://doi.org/10.1109/RadarConf2147009.2021.9455298

Kudryavtsev, V., Monzikova, A., Combot, C., Chapron, B., & Reul, N. (2019). A simplified model for the baroclinic and barotropic ocean response to moving tropical cyclones: 2. Model and simulations. *Journal of Geophysical Research: Oceans*, *124*(5), 3462–3485. https://doi.org/10.1029/2018JC014747

Kudryavtsev, V., Monzikova, A., Combot, C., Chapron, B., Reul, N., & Quilfen, Y. (2019). A simplified model for the baroclinic and barotropic ocean response to moving tropical cyclones: 1. Satellite observations. *Journal of Geophysical Research: Oceans*, *124*(5), 3446–3461. https://doi.org/10.1029/2018JC014746

Leipper, D. F. (1967). Observed Ocean conditions and hurricane Hilda, 1964. *Journal of the Atmospheric Sciences*, *24*(2), 182–186. https://doi.org/10.1175/1520-0469(1967)024⟨0182:OOCAHH⟩2.0.CO;2

Lin, I., Liu, W. T., Wu, C. C., Wong, G. T., Hu, C., Chen, Z., et al. (2003). New evidence for enhanced ocean primary production triggered by tropical cyclone. *Geophysical Research Letters*, *30*(13), 10–13. https://doi.org/10.1029/2003GL017141

Lin, S., Zhang, W.-Z., Shang, S.-P., & Hong, H.-S. (2017). Ocean response to typhoons in the western North Pacific: Composite results from Argo data. *Deep Sea Research Part I: Oceanographic Research Papers*, *123*, 62–74. https://doi.org/10.1016/j.dsr.2017.03.007

Lloyd, I. D., & Vecchi, G. A. (2011). Observational evidence for oceanic controls on hurricane intensity. *Journal of Climate*, *24*(4), 1138–1153. https://doi.org/10.1175/2010JCLI3763.1

López-Dekker, P., Biggs, J., Chapron, B., Hooper, A., Kääb, A., Masina, S., et al. (2021). The Harmony mission: End of phase-0 science overview. *International Geoscience and Remote Sensing Symposium (IGARSS)*, 7752–7755. https://doi.org/10.1109/IGARSS47720.2021.9554896

Mei, W., Lien, C.-C., Lin, I.-I., & Xie, S.-P. (2015). Tropical cyclone–induced ocean response: A comparative study of the south China sea and tropical Northwest Pacific*,+. *Journal of Climate*, *28*(15), 5952–5968. https://doi.org/10.1175/JCLI-D-14-00651.1

Moreira, A., Krieger, G., Younis, M., & Zink, M. (2023). Future spaceborne SAR technologies and mission concepts. *International geoscience and remote sensing symposium (IGARSS), 60, 2023-July, 576–578*. https://doi.org/10.1109/IGARSS52108.2023.10282219

Mouche, A., Chapron, B., Knaff, J., Zhao, Y., Zhang, B., & Combot, C. (2019). Copolarized and cross-polarized SAR measurements for high-resolution description of major hurricane wind structures: Application to Irma category 5 hurricane. *Journal of Geophysical Research: Oceans*, *124*(6), 3905–3922. https://doi.org/10.1029/2019JC015056

Mouche, A. A., Chapron, B., Zhang, B., & Husson, R. (2017). Combined Co- and cross-polarized SAR measurements under extreme wind conditions. *IEEE Transactions on Geoscience and Remote Sensing*, *55*(12), 6746–6755. https://doi.org/10.1109/TGRS.2017.2732508

Park, J. J., Kwon, Y.-O., & Price, J. F. (2011). Argo array observation of ocean heat content changes induced by tropical cyclones in the north Pacific. *Journal of Geophysical Research*, *116*(C12), C12025. https://doi.org/10.1029/2011JC007165

Perna, S., Longo, F., Zoffoli, S., Davidson, M., Iannini, L., & Lanari, R. (2024). A conceptual performance study on a two-look ScanSAR mode configuration for the forthcoming ROSE-L mission. *IEEE Transactions on Geoscience and Remote Sensing*, *62*, 1–18. https://doi.org/10.1109/TGRS.2023.3344537

Price, J. F. (1981). Upper Ocean response to a hurricane. *Journal of Physical Oceanography*, *11*(2), 153–175. https://doi.org/10.1175/1520-0485(1981)011⟨0153:UORTAH⟩2.0.CO;2

Price, J. F., Sanford, T. B., & Forristall, G. Z. (1994). Forced stage response to a moving hurricane. *CO*, *24*(2), 2–260. https://doi.org/10.1175/1520-0485(1994)024⟨0233:FSRTAM⟩2.0

Pun, I., Chang, Y. T., Lin, I. I., Tang, T. Y., & Lien, R. C. (2011). Typhoon-ocean interaction in the western North Pacific: Part 2. *Oceanography*, *24*(4), 32–41. https://doi.org/10.5670/oceanog.2011.92

Reul, N., Chapron, B., Grodsky, S. A., Guimbard, S., Kudryavtsev, V., Foltz, G. R., & Balaguru, K. (2021). Satellite observations of the sea surface salinity response to tropical cyclones. *Geophysical Research Letters*, *48*(1), 1–10. https://doi.org/10.1029/2020GL091478

Reul, N., Quilfen, Y., Chapron, B., Fournier, S., Kudryavtsev, V., & Sabia, R. (2014). Multisensor observations of the Amazon-Orinoco river plume interactions with hurricanes. *Journal of Geophysical Research: Oceans*, *119*(12), 8271–8295. https://doi.org/10.1002/2014JC010107

Roemmich, D., Alford, M. H., Claustre, H., Johnson, K. S., King, B., Moum, J., et al. (2019). On the future of Argo: A global, full-depth, multi-disciplinary array. *Frontiers in Marine Science*, *6*(JUL), 1–28. https://doi.org/10.3389/fmars.2019.00439

Roemmich, D., Johnson, G., Riser, S., Davis, R., Gilson, J., Owens, W. B., et al. (2009). The Argo program: Observing the global oceans with profiling floats. *Oceanography*, *22*(2), 34–43. https://doi.org/10.5670/oceanog.2009.36

Sampson, C. R., & Schrader, A. J. (2000). The automated tropical cyclone forecasting system (version 3.2). *Bulletin of the American Meteorological Society*, *81*(6), 1231–1240. https://doi.org/10.1175/1520-0477(2000)081⟨1231:TATCFS⟩2.3.CO;2

Sanford, T. B., Black, P. G., Haustein, J. R., Feeney, J. W., Forristall, G. Z., & Price, J. F. (1987). Ocean response to a hurricane. Part I: Observations. *Journal of Physical Oceanography*, *17*(11), 2065–2083. https://doi.org/10.1175/1520-0485(1987)017⟨2065:ORTAHP⟩2.0.CO;2

Sanford, T. B., Price, J. F., & Girton, J. B. (2011). Upper-ocean response to hurricane frances (2004) observed by profiling EM-APEX floats. *Journal of Physical Oceanography*, *41*(6), 1041–1056. https://doi.org/10.1175/2010JPO4313.1

Séguin, G., & Ahmed, S. (2009). Radarsat constellation, project objectives and status. *2009 ieee international geoscience and remote sensing symposium*, *2*, II-894-II–897. https://doi.org/10.1109/IGARSS.2009.5418242

Shay, L. K. (2009). Upper Ocean structure: Responses to strong atmospheric forcing events. *Encyclopedia of Ocean Sciences*, *1*(c), 192–210. https://doi.org/10.1016/B978-012374473-9.00628-7

Shay, L. K., & Elsberry, R. L. (1987). Near-inertial ocean current response to hurricane frederic. *Journal of Physical Oceanography*, *17*(8), 1249–1269. https://doi.org/10.1175/1520-0485(1987)017⟨1249:NIOCRT⟩2.0.CO;2

Shay, L. K., Elsberry, R. L., & Black, P. G. (1989). Vertical structure of the Ocean current response to a hurricane. *Journal of Physical Oceanography*, *19*(5), 649–669. https://doi.org/10.1175/1520-0485(1989)019⟨0649:VSOTOC⟩2.0.CO;2

Stramma, L., Cornillon, P., & Price, J. F. (1986). Satellite observations of sea surface cooling by hurricanes. *Journal of Geophysical Research*, *91*(C4), 5031–5035. https://doi.org/10.1029/JC091iC04p05031

Sun, J., Vecchi, G., & Soden, B. (2021). Sea surface salinity response to tropical cyclones based on satellite observations. *Remote Sensing*, *13*(3), 420. https://doi.org/10.3390/rs13030420

Vincent, E. M., Lengaigne, M., Madec, G., Vialard, J., Samson, G., Jourdain, N. C., et al. (2012). Processes setting the characteristics of sea surface cooling induced by tropical cyclones. *Journal of Geophysical Research*, *117*(C2). https://doi.org/10.1029/2011JC007396

Walker, N. D., Leben, R. R., Pilley, C. T., Shannon, M., Herndon, D. C., Pun, I.-F., et al. (2014). Slow translation speed causes rapid collapse of northeast Pacific Hurricane Kenneth over cold core eddy. *Geophysical Research Letters*, *41*(21), 7595–7601. https://doi.org/10.1002/2014GL061584

Wong, A. P., Wijffels, S. E., Riser, S. C., Pouliquen, S., Hosoda, S., Roemmich, D., et al. (2020). Argo data 1999–2019: Two million temperature-salinity profiles and subsurface velocity observations from a global array of profiling floats. *Frontiers in Marine Science*, *7*(July), 1–23. https://doi.org/10.3389/fmars.2020.00700

Zhang, H., Liu, X., Wu, R., Chen, D., Zhang, D., Shang, X., et al. (2020). Sea surface current response patterns to tropical cyclones. *Journal of Marine Systems*, *208*(February), 103345. https://doi.org/10.1016/j.jmarsys.2020.103345

Zhang, J., Lin, Y., Chavas, D. R., & Mei, W. (2019). Tropical cyclone cold wake size and its applications to power dissipation and ocean heat uptake estimates. *Geophysical Research Letters*, *46*(16), 10177–10185. https://doi.org/10.1029/2019GL083783